

Enhanced Maximum Independent Set Preparation with Rydberg Atoms Guided by the Spectral Gap

Seokho Jeong  and Minhyuk Kim *

Department of Physics, Korea University, Seoul 02841, Republic of Korea

(Dated: February 23, 2026)

Adiabatic quantum computation with Rydberg atoms provides a natural route for solving combinatorial optimization problems such as the maximum independent set (MIS). However, its performance is fundamentally limited by the reduction of the spectral gap with increasing system size and connectivity, which induces population leakage from the ground state during finite-time evolution. Here we introduce the Adjusted Detuning for Ground-Energy Leakage Blockade (ADGLB), a spectral-gap-guided schedule engineering method that modifies the laser detuning profile to suppress leakage without introducing additional Hamiltonian terms or iterative optimization loops. We experimentally benchmark ADGLB on a quasi-one-dimensional chain of $N = 10$ atoms, and the MIS preparation probability increases substantially compared with the standard adiabatic schedule. Furthermore, we show that the schedule optimized for smaller instances can be directly applied to larger two-dimensional triangular lattices with $N = 25$ and $N = 37$. With a small heuristic offset, the method also remains effective for instances with higher hardness parameters. These findings demonstrate that spectral-gap-guided schedule engineering offers a scalable and hardware-efficient strategy for enhancing adiabatic quantum optimization on neutral-atom platforms.

I. INTRODUCTION

Over the past few decades, advances in the experimental control of quantum systems have brought quantum information processing closer to practical relevance [1–5]. Both analog and digital approaches to quantum evolution have been actively explored, enabling applications in combinatorial optimization [6–14], quantum simulation of many-body physics [15–22], and quantum error correction [23–28]. These developments have been implemented across promising platforms such as trapped ions [9, 10, 19–22, 27, 28], superconducting circuits [11, 12, 17, 18, 24, 25, 29], and neutral atoms [13–16, 23, 26].

Among these platforms, Rydberg-atom arrays combine flexible programmability with intrinsic scalability [30]. Strong, distance-dependent Rydberg interactions naturally induce entanglement between nearby atoms [31, 32], while site-resolved laser control enables the implementation of tunable many-body Hamiltonians and programmable unitary dynamics [33, 34]. These capabilities have established Rydberg systems as a versatile platform for quantum optimization and simulation [33–36].

The maximum independent set (MIS) problem provides a particularly accessible application of adiabatic quantum computing (AQC) in Rydberg-atom platforms, offering a physically intuitive scheme in which solutions are encoded in the ground state of a gradually evolving Hamiltonian [6, 7]. This problem can be encoded naturally using Rydberg blockade, where constraints arise directly from interaction-induced energy penalties [13, 14, 37, 38]. Recent experiments have demonstrated MIS

on instances with various connectivity structures and extended this approach to broader classes of optimization problems through MIS mappings [13, 14, 37–46].

Despite these advances, the performance of AQC remains fundamentally constrained. In particular, the minimum spectral gap typically decreases with increasing system size and depends sensitively on the problem instance, thereby leading to population leakage from the ground state for a finite evolution time [47–49]. Consequently, designing the adiabatic evolution under a fixed total evolution time is crucial. This limitation is closely related to the instantaneous spectral properties of the system; however, accessing this information for large-scale quantum Hamiltonians remains challenging.

Alternative approaches include analog counterdiabatic quantum computing [50–52], which typically requires additional Hamiltonian terms. Variational algorithms and Bayesian optimization [53] rely on repeated circuit executions and extensive sampling, leading to substantial hardware overhead. Classical post-processing and mitigation techniques can partially improve performance, but their effectiveness ultimately depends on the quality of the probability distributions produced by the quantum hardware.

In this work, we demonstrate an enhancement in MIS preparation guided by the spectral gap. We introduce the Adjusted Detuning for Ground-Energy Leakage Blockade (ADGLB) method, which leverages an analytical approach to design a laser-detuning sweep schedule based on the spectral gap, without introducing additional Hamiltonian terms, thereby suppressing ground-state population leakage. We validate this approach on k -PXP chain-type arrangements, which represent relatively hard instances among problems of comparable size [54]. While direct investigation of the spectral gap is feasible only for small instances, we further show that the

* minhyukkim@korea.ac.kr

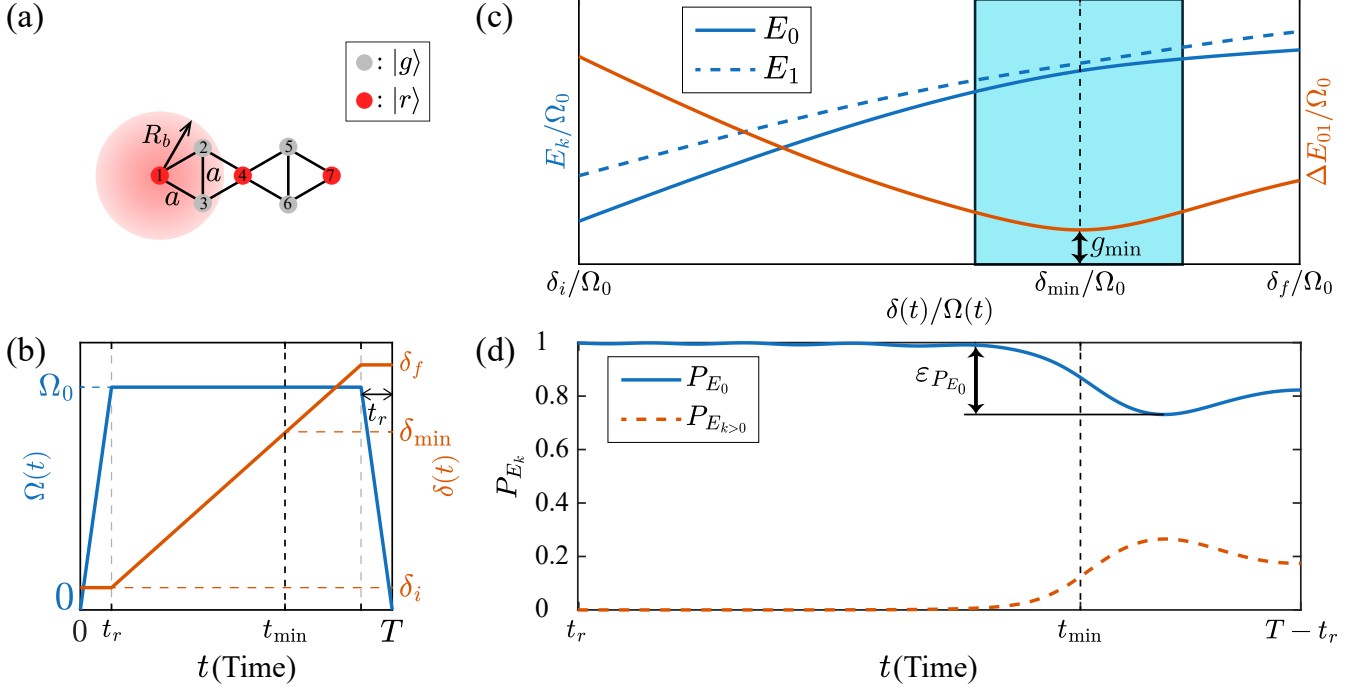


FIG. 1. AQC for MIS preparation with Rydberg atoms. (a) An example of a MIS encoded in a $N = 7$ Rydberg-atom array with nearest-neighbor spacing a , where atoms within the Rydberg blockade radius R_b cannot be simultaneously excited. The atomic ground state $|g\rangle$ and the Rydberg state $|r\rangle$ are represented by gray and red circles, respectively. (b) The standard AQC schedule of the Rabi frequency $\Omega(t)$ and the detuning $\delta(t)$. (c) The ground-state energy E_0 (blue solid line), the first excited-state energy E_1 (blue dashed line), and the spectral gap $\Delta E_{01} \equiv E_1 - E_0$ (red solid line) as a function of the detuning $\delta(t)$ during the linear sweep ($t_r \leq t \leq T - t_r$) of the standard schedule shown in (b). The region around the minimum spectral gap $g_{\min} \equiv \min_{t \in [0, T]} \Delta E_{01}(t)$ near δ_{\min} is highlighted in light blue. (d) The time evolution of the ground-state population P_{E_0} (blue solid line) and the population of all excited states $P_{E_{k>0}} \equiv 1 - P_{E_0}$ (red dashed line). The population leakage from the ground state is denoted by $\varepsilon_{P_{E_0}}$.

optimized schedule can be directly applied to larger instances with similar hardness, as well as to harder instances through modest adjustments of the schedule.

The remainder of this paper is organized as follows. In Sec. II, we introduce the theoretical background of adiabatic quantum computing with Rydberg Hamiltonians for MIS preparation along with the ADGLB-based method for scheduling laser detuning. In Sec. III, we present experimental validations of the ADGLB method, and in Sec. IV, we discuss its applicability to more complex problem instances. The conclusions are given in Sec. V.

II. THEORETICAL CONSIDERATION

A. AQC for Rydberg MIS

Figure 1(a) describes an array of $N = 7$ Rydberg atoms. Each atom spans a two-level system of the atomic ground state $|g\rangle$ and the Rydberg state $|r\rangle$. When the distance a between adjacent atoms is smaller than R_b (blockade radius), Rydberg blockade occurs, i.e. only one atom can

be excited to the Rydberg state $|r\rangle$ under the illumination of a laser. The Hamiltonian H_{Ry} of such Rydberg atom systems is given by

$$H_{\text{Ry}}(t) = \sum_{v \in V} \left[\frac{\Omega(t)}{2} \sigma_x^{(v)} + \frac{\delta(t)}{2} \sigma_z^{(v)} \right] + U \sum_{(u,v) \in E} n_u n_v, \quad (1)$$

where Ω is the Rabi frequency of the laser coupling between $|g\rangle$ and $|r\rangle$, δ is the laser detuning, U is the van der Waals interaction between two Rydberg atoms of $U = C_6/a^6$ with coefficient C_6 and the interatomic distance a , and $n_v \equiv |r\rangle_v \langle r|_v$, $\sigma_x^{(v)} \equiv |r\rangle_v \langle g|_v + |g\rangle_v \langle r|_v$ and $\sigma_z^{(v)} \equiv |g\rangle_v \langle g|_v - |r\rangle_v \langle r|_v$ ($= 1 - 2n_v$) are the excitation number and Pauli- x, z matrices of the node v . The Rydberg blockade condition is satisfied when $\Omega \ll U$ so that the blockade radius gives that $R_b = (C_6/\Omega)^{1/6}$. The MIS state is given by the lowest-energy eigenstate (ground state) of the Rydberg Hamiltonian H_{Ry} with $\Omega = 0$ and $0 < \delta < U$.

The standard adiabatic evolution schedule for the Rydberg MIS is illustrated in Fig. 1 (b). Starting from the initial state where all atoms are in $|g\rangle$ (the ground state of H_{Ry} with $\Omega = 0$ and $\delta = \delta_i < 0$), the standard adiabatic

schedule consists of the following three stages:

- (i) The Rabi frequency is ramped up from zero to Ω_0 during the time interval $0 \leq t < t_r$.
- (ii) While the Rabi frequency is maintained at Ω_0 , the detuning δ is swept from $\delta_i < 0$ to $0 < \delta_f < U$, during $t_r \leq t < T - t_r$.
- (iii) The Rabi frequency is ramped down from Ω_0 to zero during $T - t_r \leq t \leq T$.

If the evolution under the above schedule is sufficiently adiabatic, the system is always populated in the ground state and reaches the MIS state.

We study the eigenenergy structure and population change for the $N = 7$ Rydberg atom array under the standard adiabatic evolution schedule, as in Fig. 1 (c-d). The ground-state energy E_0 , the first excited-state energy E_1 , and spectral gap $\Delta E_{01} (\equiv E_1 - E_0)$ are depicted in Fig. 1 (c). In the highlighted region in Fig. 1(c), the energy gap ΔE_{01} becomes small compared to the other regions and is minimized at $t = t_{\min}$ with $\delta_{\min} = \delta(t_{\min})$. In this region, the population P_{E_0} in the ground state starts to leak to higher eigenenergy states, as in Fig. 1(d). Then the amount of leakage is $\varepsilon_{P_{E_0}}$.

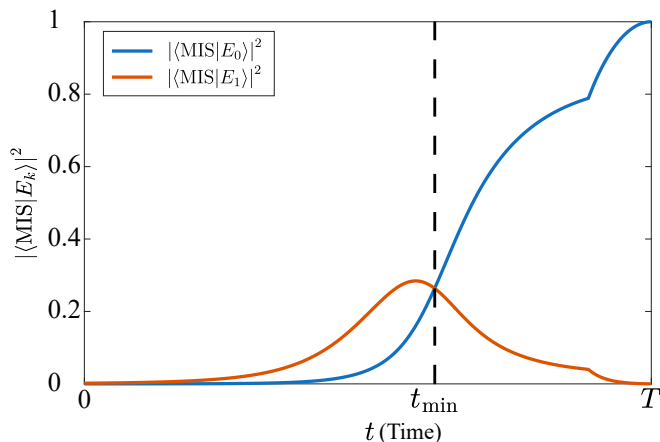


FIG. 2. MIS-state overlaps $|\langle \text{MIS} | E_k \rangle|^2$ with the ground state (blue line) and the first excited state (red line) for the $N = 7$ Rydberg atom array in Fig. 1(a) along the standard AQC schedule.

The dynamics of the MIS-state overlap $|\langle \text{MIS} | E_k \rangle|^2$ with the ground state, and the first excited state is depicted in Fig. 2. In this example, the MIS state is given by $|\text{MIS}\rangle = |rggrggr\rangle$. Although the MIS state perfectly overlaps the ground state at the end of the schedule, mixing between the MIS state and the first excited state occurs near $t = t_{\min}$. Consequently, population leakage $\varepsilon_{P_{E_0}}$ from the ground state directly results in infidelity in MIS preparation under the linear detuning schedule $\delta(t)$, indicating that a careful modification of $\delta(t)$ near t_{\min} is required.

For arrangements of the same size, more complex connectivity between Rydberg atoms leads to more complex eigenspectrum structures and a reduced minimum spectral gap $g_{\min} \equiv \min_{t \in [0, T]} \Delta E_{01}(t)$, thereby enhancing population leakage from the ground state. Moreover, as the system size increases, the minimum spectral gap g_{\min} decreases superexponentially [47]. The performance of the AQC for a given arrangement can be characterized by the hardness parameter $\text{HP} = R_{|\text{MIS}\rangle-1} / (|\text{MIS}\rangle R_{|\text{MIS}\rangle})$, where R_k denotes the number of independent sets of size k . As a result, the required adiabatic duration T increases for more complex or harder instances, competing with the finite coherence time of the quantum hardware. In the following subsection, we introduce a method to enhance Rydberg AQC performance by exploiting the structural features of the eigenspectrum. We further experimentally demonstrate that a schedule optimized for small instances can be extended to larger arrangements.

B. Adjusted Detuning for Ground-energy Leakage Blockade (ADGLB)

The dominant contribution to infidelity in MIS preparation arises from population leakage from the ground state $|E_0\rangle$ to the first excited state $|E_1\rangle$. We therefore consider an effective two-level adiabatic Hamiltonian H_{ad} defined within the reduced subspace $\{|E_0\rangle, |E_1\rangle\}$:

$$H_{\text{ad}} = \frac{\langle E_1 | \frac{dH_{\text{Ry}}}{dt} | E_0 \rangle}{\Delta E_{01}} s_y - \frac{\Delta E_{01}}{2} s_z, \quad (2)$$

where $s_y \equiv i|E_1\rangle\langle E_0| - i|E_0\rangle\langle E_1|$ and $s_z \equiv |E_0\rangle\langle E_0| - |E_1\rangle\langle E_1|$ are the Pauli- y and Pauli- z operators in the basis $\{|E_0\rangle, |E_1\rangle\}$, respectively (See Appendix for details). The time evolution of the amplitudes $|E_0\rangle$ and $|E_1\rangle$ follows from the Schrödinger equation:

$$i \begin{pmatrix} \dot{c}_0 \\ \dot{c}_1 \end{pmatrix} = H_{\text{ad}} \cdot \begin{pmatrix} c_0 \\ c_1 \end{pmatrix}, \quad (3)$$

where c_j denotes the probability amplitude of $|E_j\rangle$ -state ($j = 0, 1$), with $P_{E_j} = |c_j|^2$, and $\dot{c}_j \equiv (dc_j/dt)$ its time-derivative.

In the adiabatic Hamiltonian of Eq. (2), the off-diagonal term represents the coupling between $|E_0\rangle$ and $|E_1\rangle$, which induces population leakage from the ground state. Therefore, the coupling term should remain sufficiently small compared to the energy splitting during adiabatic evolution to suppress nonadiabatic transitions. For a fixed evolution time T , the spectral gap ΔE_{01} varies with time and reaches its minimum g_{\min} . To maintain adiabaticity under this constraint, the rate of change dH_{Ry}/dt should be reduced in the vicinity of g_{\min} , while it can be increased away from this region compared to the standard schedule. Motivated by this principle, we introduce Adjusted Detuning for Ground-energy Leakage

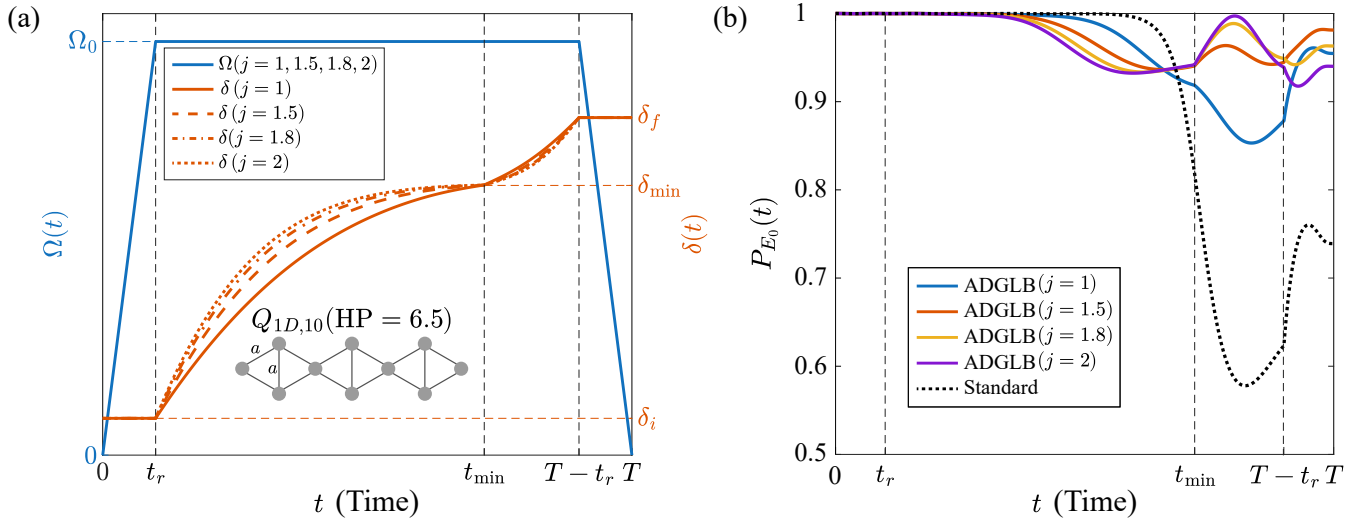


FIG. 3. (a) The ADGLB schedule constructed using Eqs. (4) and (5) with $j = 1, 1.5, 1.8, 2$, for a quasi-one-dimensional chain of $N = 10$ Rydberg atoms, $Q_{1D,10}$ (HP = 6.5). (b) Numerical results for the ground-state population dynamics $P_{E_0}(t)$ under the standard schedule (black dashed line) and the ADGLB schedules with $j = 1$ (blue solid line), 1.5 (red solid line), 1.8 (yellow solid line), and 2 (purple solid line).

Blockade (ADGLB), a method that modifies the laser-detuning schedule $\delta(t)$ to suppress ground-state leakage. The detailed procedure is described below.

The design of the modified detuning schedule $\delta(t)$ is inspired by the theorem that population leakage $\varepsilon_{P_{E_0}}$ is bounded by the evolution time and inverse power of the spectral gap, $(\Delta E_{01})^{-j}$ [47]. In ADGLB, the Rabi frequency schedule $\Omega(t)$ is kept identical to the standard schedule, while only the detuning $\delta(t)$ is modified within the time interval where the Rabi frequency reaches its maximum value Ω_0 ($t_r < t < T - t_r$), because the spectral gap ΔE_{01} is proportional to Ω_0 . The detuning is designed such that its time derivative satisfies $d\delta/dt \propto (\Delta E_{01}(t))^j$. The interval is split into two segments at t_{\min} , where $\Delta E_{01}(t)$ reaches its minimum value g_{\min} (at δ_{\min}). The detuning path $\delta(t)$ is then constructed using a normalized interpolation function defined as

$$\zeta_j(t, t_0, t_1) \equiv \frac{\int_{t_0}^t dt' \cdot [\Delta E_{01}(t')]^j}{\int_{t_0}^{t_1} dt' \cdot [\Delta E_{01}(t')]^j} \quad (t_0 \leq t \leq t_1, j > 0). \quad (4)$$

Therefore, the complete detuning schedule is given by

$$\delta(t) = \begin{cases} \delta_i & 0 \leq t \leq t_r, \\ \delta_i + (\delta_{\min} - \delta_i) \cdot \zeta_j(t, t_r, t_{\min}) & t_r \leq t \leq t_{\min}, \\ \delta_{\min} + (\delta_f - \delta_{\min}) \cdot \zeta_j(t, t_{\min}, T - t_r) & t_{\min} \leq t \leq T - t_r, \\ \delta_f & T - t_r \leq t \leq T. \end{cases} \quad (5)$$

We tested ADGLB on a quasi-one-dimensional chain of Rydberg atoms, referred to as the k -PXP geometry [54], whose configuration is shown in Fig. 3(a). This

geometry exhibits a large number of independent sets of size $|\text{MIS}| - 1$, $R_{|\text{MIS}|-1}$, relative to the number of maximum independent sets $R_{|\text{MIS}|}$, resulting in a comparatively large hardness parameter HP among arrangements of similar size. Moreover, the triangular geometry provides a clear separation between nearest- and next-nearest-neighbor interactions, which are well described by Eq. (1). As an example, we determine the modified detuning schedule $\delta(t)$ for a $N = 10$ quasi-one-dimensional Rydberg chain, $Q_{1D,10}$, using Eqs. (4) and (5). The resulting ADGLB schedules for several values of j in the range $1 \leq j \leq 2$ are shown in Fig. 3(a).

We compared the ground-state population P_{E_0} under the standard and ADGLB schedules through numerical calculations of the Schrödinger equation with the Hamiltonian in Eq. (1), as shown in Fig. 3(b). While the final ground-state population for the standard schedule was $P_{E_0} = 0.739$, the ADGLB schedules yielded $P_{E_0} > 0.94$. Specifically, for $j = 1, 1.5, 1.8$, and 2, the corresponding values were 0.955, 0.981, 0.963, and 0.940, respectively. Here, the parameter j controls the strength of the schedule modification near the minimum spectral gap. An intermediate value around $j = 1.5$ provides the highest performance, reflecting a balance between sufficient slow-down near g_{\min} and avoiding excessive distortion of the overall evolution.

III. RESULTS

To benchmark ADGLB, we performed experiments on MIS instances using QuEra's Aquila neutral-atom processor [55], accessed via the Amazon Braket service. The laser pulse excites ^{87}Rb atoms from the atomic ground

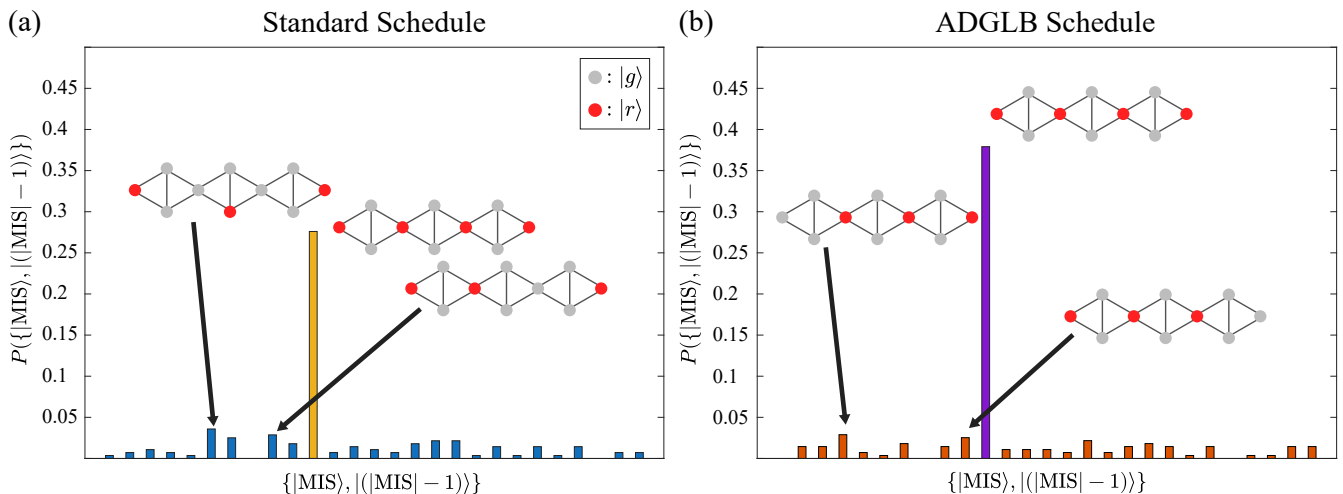


FIG. 4. Experimental MIS preparation for the quasi-one-dimensional chain $Q_{1D,10}$. (a) Probability histogram of independent sets of size $|MIS|$ (yellow bar) and $|MIS| - 1$ (blue bars) under the standard schedule (279 valid shots). (b) Probability histogram of independent sets of size $|MIS|$ (yellow bar) and $|MIS| - 1$ (blue bars) under the ADGLB schedule with $j = 1.8$ (277 valid shots).

state $|g\rangle = |5S_{1/2}\rangle$ to the Rydberg state $|r\rangle = |70S_{1/2}\rangle$, characterized by a van der Waals interaction coefficient $C_6 = 2\pi \times 863 \text{ GHz} \cdot \mu\text{m}^6$. The pulse has a peak Rabi frequency $\Omega_0 = 2\pi \times 1.0 \text{ MHz}$ and sweeps the detuning from $\delta_i = 2\pi \times (-2.5) \text{ MHz}$ to $\delta_f = 2\pi \times (+2.5) \text{ MHz}$. The nearest-neighbor spacing was $a = 8 \mu\text{m}$, yielding an interaction strength $U = 2\pi \times 3.29 \text{ MHz}$. Under the condition $\delta_f < U$, the MIS configuration corresponds to the ground state of the Rydberg Hamiltonian in Eq. (1). The ADGLB detuning schedule was implemented with a power exponent $j = 1.8$ using Eqs. (4) and (5). For all experiments, the total adiabatic evolution time was $T = 5 \mu\text{s}$ with a ramp time $t_r = 0.5 \mu\text{s}$. For the arrangement $Q_{1D,10}$, the minimum-gap parameters are $(t_{\min}, \delta_{\min}, g_{\min}) = (3.60 \mu\text{s}, 2\pi \times 1.38 \text{ MHz}, 2\pi \times 0.29 \text{ MHz})$.

A. Experimental enhancement of MIS preparation in a quasi-one-dimensional chain

We now compare the experimental MIS preparation probabilities under the standard and ADGLB schedules. Figure 4 shows the experimental probability histograms of independent sets of size $|MIS|$ and $|MIS| - 1$ for the quasi-one-dimensional chain $Q_{1D,10}$ (HP = 6.5), obtained under the standard schedule and the ADGLB schedule with $j = 1.8$. The probability of MIS preparation, P_{MIS} , increases from 28% under the standard schedule to 38% under the ADGLB schedule. Each experiment was repeated 300 times, and the number of valid shots corresponding to defect-free atomic arrays was 279 and 277 for the standard and ADGLB schedules, respectively.

The discrepancy between the numerical results and the experimental observations can be primarily attributed

to experimental imperfections of the hardware. These include state-preparation-and-measurement (SPAM) errors of $P(g|r) = 10.0\%$ and $P(r|g) = 5.0\%$, a detuning error of $(2\pi) \times 160 \text{ kHz}$, and a coherence time of $8 \mu\text{s}$ (measured via Rabi oscillations), limited by residual phase noise of the Rydberg excitation lasers [56]. Due to these imperfections, the differences in $P(\text{MIS})$ among the ADGLB schedules with different j are not experimentally resolved; however, they remain clearly higher than the probability obtained under the standard schedule.

B. Experimental enhancement of MIS preparation in two-dimensional triangular lattices

We demonstrated that the optimal schedule obtained via ADGLB for a quasi-one-dimensional chain can be directly adapted to larger arrangements with similar geometric structures. Figures 5(a) and (c) present diamond-shaped and hexagonal-shaped triangular lattice instances, $T_{D,25}$ ($N = 25$, HP = 6.16, $|MIS| = 9$) and $T_{H,37}$ ($N = 37$, HP = 5.38, $|MIS| = 13$), respectively, for which direct diagonalization of the spectral structure becomes computationally demanding. These lattices were constructed by stacking triangular building blocks of the quasi-one-dimensional chain along the perpendicular direction (see Table II in Appendix A for atomic coordinates). This extension provides a more stringent test of leakage suppression near the minimum spectral gap, owing to the increased connectivity and larger number of $|MIS| - 1$ configurations.

Both instances have HP values similar to those of the quasi-one-dimensional chain $Q_{1D,10}$. The experimental probability histograms for $T_{D,25}$ and $T_{H,37}$ are shown in Fig. 5(b) and (d), respectively. The upper panels cor-

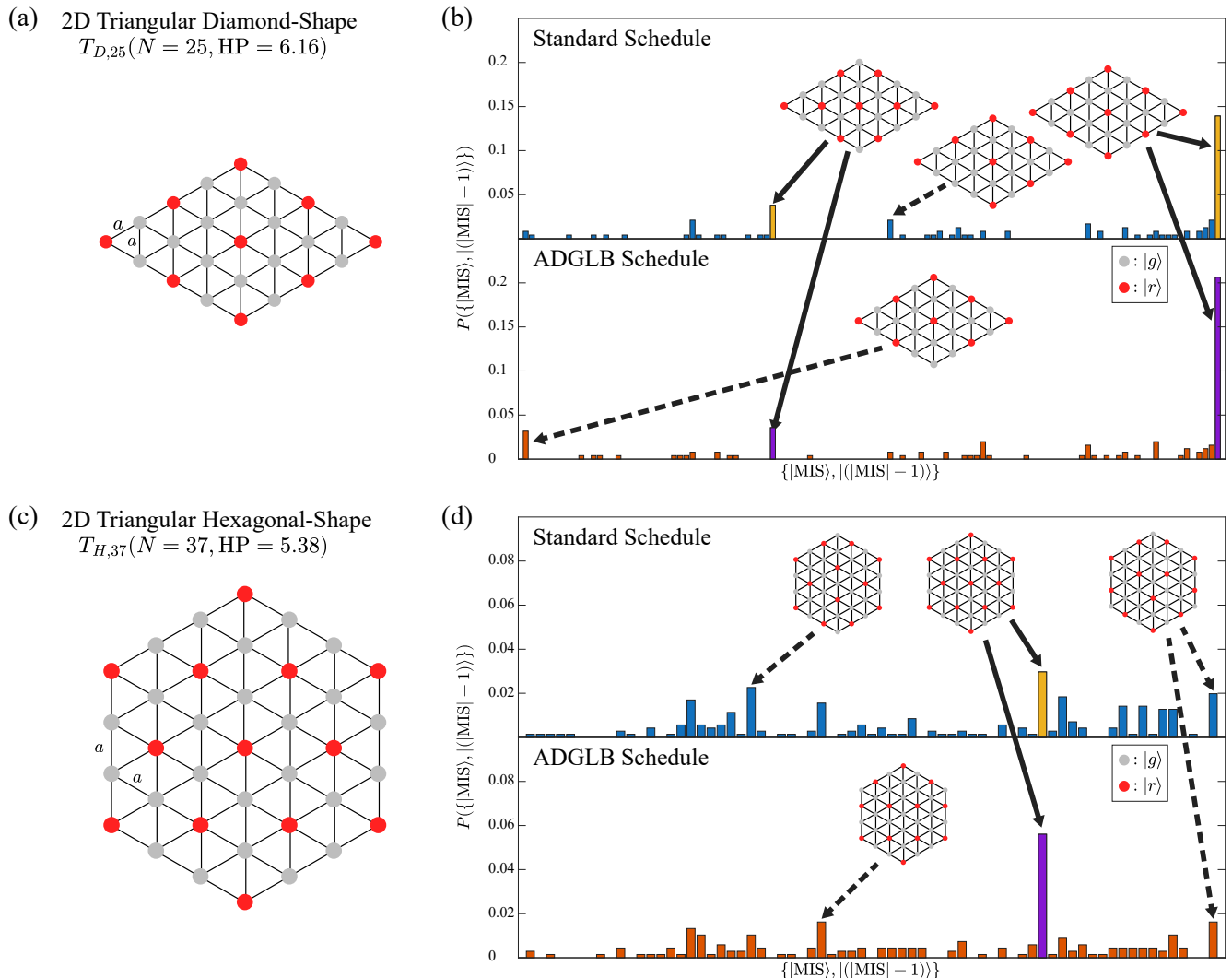


FIG. 5. Experimental MIS preparation in two-dimensional triangular lattices. (a) A two-dimensional diamond-shaped lattice $T_{D,25}$. (b) Probability histograms of independent sets of size $|\text{MIS}|$ and $|\text{MIS}| - 1$ for $T_{D,25}$ under the standard (237 valid shots) and ADGLB (252 valid shots) schedules. (c) A two-dimensional hexagonal-shaped lattice $T_{H,37}$. (d) Probability histograms of independent sets of size $|\text{MIS}|$ and $|\text{MIS}| - 1$ for $T_{D,25}$ under the standard (707 valid shots) and ADGLB (678 valid shots) schedules. In (b) and (d), yellow and purple bars denote independent sets of size $|\text{MIS}|$, while blue and red bars denote independent sets of size $|\text{MIS}| - 1$.

respond to the standard schedule, while the lower panels correspond to the ADGLB schedule, using the same schedule as applied in Fig. 4. For $T_{D,25}$, the MIS preparation probability P_{MIS} increased from 17.7% under the standard schedule to 24.2% under the ADGLB schedule (yellow and purple bars in Fig. 5(b), respectively). For $T_{H,37}$, P_{MIS} increased from 3.0% to 5.6%. The number of valid shots was 252 (standard: 237) for $T_{D,25}$ and 678 (standard: 707) for $T_{H,37}$.

Overall, these results suggest that schedules optimized using ADGLB for smaller instances can be transferred to larger systems with comparable hardness characteristics. Despite the increased system size and connectivity, applying the same schedule enhances MIS preparation

without requiring additional experimental resources or a longer AQC duration. This indicates that the spectral-gap-guided schedule modification effectively reflects the structural features associated with instance hardness rather than merely the system size.

IV. DISCUSSION: EXTENSION TO HIGHER-HARDNESS ARRANGEMENTS

Now we discuss the applicability of the optimized schedule via ADGLB to larger hardness parameter instances. We investigated the typical behavior of the eigenenergy spectra for quasi-one-dimensional arrangements of vari-

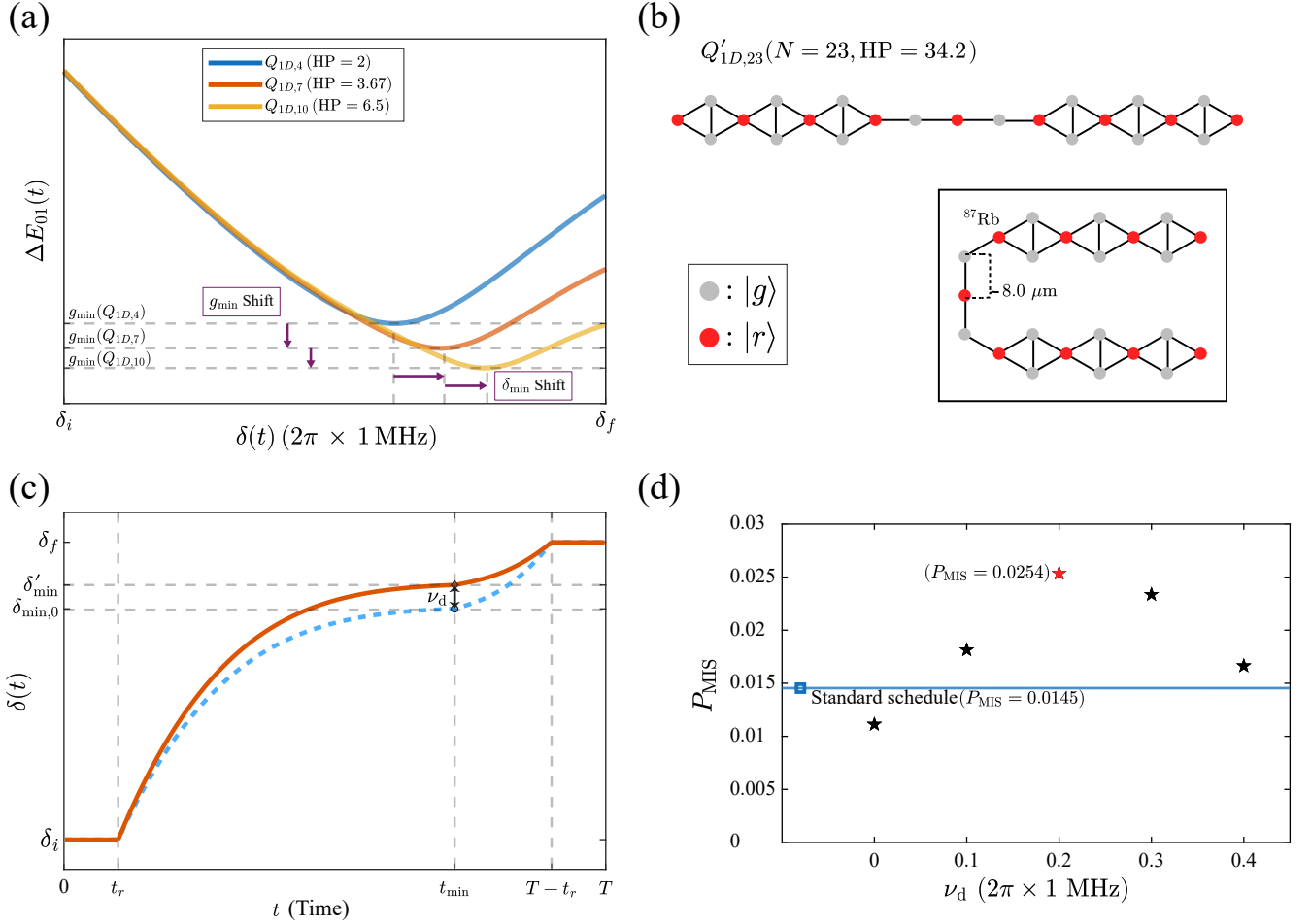


FIG. 6. Extension to higher hardness arrangements. (a) The spectral gaps $\Delta E_{01}(t)$ for three quasi-one-dimensional chains with sizes $N = 4, 7, 10$ ($Q_{1D,4}$, $Q_{1D,7}$, and $Q_{1D,10}$ with $HP = 2, 3.67$, and 6.5 , respectively). As N and HP increase, the minimum spectral gaps $g_{\min}(Q_{1D,4})$, $g_{\min}(Q_{1D,7})$, and $g_{\min}(Q_{1D,10})$ decrease, while the corresponding detuning values δ_{\min} increase. (b) A quasi-one-dimensional chain $Q'_{1D,23}$, consisting of two $Q_{1D,10}$ arrangements connected by a linear atomic chain. The inset depicts the experimental geometry. (c) The ADGLB schedule for $Q'_{1D,23}$ (red solid line), modified from the ADGLB schedule for $Q_{1D,10}$ (blue dashed line) with a heuristic offset ν_d . (d) MIS preparation probability P_{MIS} for $Q'_{1D,23}$ with different heuristic offsets ν_d . The blue solid line denotes P_{MIS} under the standard schedule ($P_{\text{MIS}} = 0.0145$). The red star denotes the maximum MIS preparation probability. The number of valid shots were 894, 899, 882, 907, 899, and 902 for the standard schedule and the modified ADGLB schedules with $\nu_d = 0, 0.1, 0.2, 0.3$, and 0.4 , respectively.

ous sizes. In Fig. 6(a), the spectral gaps $\Delta E_{01}(t)$ for arrangements $Q_{1D,4}$, $Q_{1D,7}$, and $Q_{1D,10}$ are shown according to the standard schedule. Not only does the minimum spectral gap g_{\min} decrease for larger hardness parameters, but the corresponding δ_{\min} also tends to increase.

We show that the schedule optimized via ADGLB for a small-sized, low-hardness arrangement can be applied to a harder arrangement with only a simple modification. As an example, we consider an arrangement $Q'_{1D,23}$ in which it consists of two $Q_{1D,10}$ arrangements connected by a 1D linear atomic chain, as in Fig. 6(b). The hardness parameter of the arrangement is $HP = 34.2$, and it is a relatively hard instance with a similar size N compared to the previous two-dimensional triangular lattices. And it is very daunting to estimate δ_{\min} by directly diagonalizing

its Hamiltonian matrix.

Guided by the tendency that δ_{\min} increases for arrangements with a larger size or HP , we estimate the detuning corresponding to the spectral gap $g_{\min}(Q'_{1D,23})$ by modifying the adiabatic evolution schedule optimized by the ADGLB in the previous section. At t_{\min} , we define a modified detuning $\delta'_{\min} = \delta_{\min,0} + \nu_d$, where ν_d denotes a heuristic offset. The entire modified detuning schedule is given by

$$\delta(t; \delta'_{\min}) = \begin{cases} \delta_i + \frac{\delta'_{\min} - \delta_i}{\delta_{\min,0} - \delta_i} \cdot \eta_A (t - t_r) & t_r \leq t \leq t_{\min}, \\ \delta'_{\min} + \frac{\delta_f - \delta'_{\min}}{\delta_f - \delta_{\min,0}} \cdot \eta_B (t - t_{\min}) & t_{\min} \leq t \leq T - t_r. \end{cases} \quad (6)$$

Here, $\eta_A(s)$ and $\eta_B(s)$ are polynomial approximations of the ADGLB schedule optimized with the $Q_{1D,10}$, expressed as:

$$\eta_A(s) \equiv 4.0047s - 1.5785s^2 + 0.2826s^3 - 0.0193s^4 \quad (7a)$$

$$\eta_B(s) \equiv 0.5509s - 0.055s^2 + 1.4402s^3 - 0.565s^4, \quad (7b)$$

with a generalized time s . The ADGLB and modified detuning schedule $\delta(t)$ are depicted in Fig. 6(c) (blue dashed and red solid lines), respectively.

Fig. 6 (d) shows the experimental MIS preparation probability P_{MIS} for five different adiabatic evolution schedules defined by Eq. (6), with different values of the heuristic offset $\nu_d = 2\pi \times \{0, 0.1, 0.2, 0.3, 0.4\}$ MHz. When $\nu_d = 0$, we find $P_{\text{MIS}} = 0.011$, which is smaller than the result obtained using the standard adiabatic evolution schedule ($P_{\text{MIS}} = 0.0145$, blue line), suggesting that the ADGLB schedule optimized for a small-size arrangement may not be well matched to the eigenenergy structure of larger arrangements. However, as ν_d increases, P_{MIS} is enhanced and reaches its maximum value of 0.0254 at $\nu_d = 2\pi \times 0.2$ MHz, exceeding the result of the standard adiabatic evolution schedule. The enhancement of P_{MIS} for a finite heuristic offset ν_d indicates that a slight modification of the detuning near t_{min} can improve adiabatic evolution near the minimum spectral gap.

V. CONCLUSION

In summary, we developed a method to enhance MIS preparation in Rydberg-atom adiabatic quantum computations. The proposed ADGLB method leverages the spectral gap of the Rydberg Hamiltonian to modify the laser-detuning schedule, thereby suppressing the population leakage from the ground state without introducing additional Hamiltonian terms. We determined an optimized detuning schedule for a quasi-one-dimensional

chain of $N = 10$ Rydberg atoms, which exhibits a relatively large hardness parameter HP compared to arrangements of similar size. The experimental results confirmed that the MIS preparation probability was significantly enhanced relative to the standard schedule. Furthermore, we demonstrated that the same ADGLB schedule optimized for the quasi-one-dimensional chain can be directly applied to two-dimensional triangular lattices with $N = 25$ and $N = 37$, which possess larger system sizes but comparable hardness parameters. In addition, by introducing a heuristic offset to the ADGLB schedule optimized for smaller systems, the method remains effective for instances with higher hardness, including a quasi-one-dimensional chain with $N = 23$ and $\text{HP} = 34.2$.

Overall, the spectral-gap-guided schedule modification improved adiabatic performance without requiring repeated use of quantum hardware or complex control terms. By enhancing the quality of the probability distribution generated at the hardware level, this approach may also facilitate classical post-processing and error-mitigation strategies in AQC.

ACKNOWLEDGMENTS

This research was supported by the National Research Foundation of Korea (NRF) under Grant Nos. RS-2024-00337653 and RS-2025-25464441, funded by the Korea government (MSIT).

DATA AVAILABILITY

The data that support the findings of this study are available from the corresponding author upon reasonable request.

CONFLICTS OF INTEREST

The authors declare no conflict of interest.

-
- [1] R. P. Feynman, Simulating physics with computers, *Int. J. Theor. Phys.* **21**, 467 (1982).
 - [2] M. A. Nielsen and I. L. Chuang, *Quantum computation and quantum information* (Cambridge university press, 2010).
 - [3] A. G. J. MacFarlane, J. P. Dowling, and G. J. Milburn, Quantum technology: the second quantum revolution, *Philos. Trans. A. Math. Phys. and Eng. Sci.* **361**, 1655 (2003).
 - [4] P. Shor, Algorithms for quantum computation: discrete logarithms and factoring, in *Proc. 35th Ann. Symp. on Foundations of Computer Science* (1994) pp. 124–134.
 - [5] L. K. Grover, Quantum mechanics helps in searching for a needle in a haystack, *Phys. Rev. Lett.* **79**, 325 (1997).
 - [6] E. Farhi, J. Goldstone, S. Gutmann, J. Lapan, A. Lundgren, and D. Preda, A quantum adiabatic evolution algorithm applied to random instances of an np-complete problem, *Science* **292**, 472 (2001).
 - [7] N. G. Dickson and M. H. S. Amin, Does adiabatic quantum optimization fail for np-complete problems?, *Phys. Rev. Lett.* **106**, 050502 (2011).
 - [8] V. Choi, Adiabatic quantum algorithms for the np-complete maximum-weight independent set, exact cover and 3sat problems (2010), arXiv:1004.2226.
 - [9] P. Niroula, R. Shaydulin, R. Yalovetzky, P. Minssen, D. Herman, S. Hu, *et al.*, Constrained quantum optimization for extractive summarization on a trapped-ion quantum computer, *Sci. Rep.* **12**, 17171 (2022).

- [10] Y. Zhu, Z. Zhang, B. Sundar, A. M. Green, C. Huerta Alderete, N. H. Nguyen, *et al.*, Multi-round qaoa and advanced mixers on a trapped-ion quantum computer, *Quantum Sci. Technol.* **8**, 015007 (2022).
- [11] M. Dupont, B. Evert, M. J. Hodson, B. Sundar, S. Jeffrey, Y. Yamaguchi, *et al.*, Quantum-enhanced greedy combinatorial optimization solver, *Sci. Adv.* **9**, eadi0487 (2023).
- [12] M. Dupont, B. Sundar, B. Evert, D. E. B. Neira, Z. Peng, S. Jeffrey, *et al.*, Benchmarking quantum optimization for the maximum-cut problem on a superconducting quantum computer, *Phys. Rev. Appl.* **23**, 014045 (2025).
- [13] S. Jeong, M. Kim, M. Hhan, J. Park, and J. Ahn, Quantum programming of the satisfiability problem with rydberg atom graphs, *Phys. Rev. Res.* **5**, 043037 (2023).
- [14] S. Ebadi, A. Keesling, M. Cain, T. T. Wang, H. Levine, D. Bluvstein, *et al.*, Quantum optimization of maximum independent set using rydberg atom arrays, *Science* **376**, 1209 (2022).
- [15] S. Ebadi, T. T. Wang, H. Levine, A. Keesling, G. Semeghini, A. Omran, *et al.*, Quantum phases of matter on a 256-atom programmable quantum simulator, *Nature* **595**, 227 (2021).
- [16] S. de Léséleuc, V. Lienhard, P. Scholl, D. Barredo, S. Weber, N. Lang, *et al.*, Observation of a symmetry-protected topological phase of interacting bosons with rydberg atoms, *Science* **365**, 775 (2019).
- [17] X. Zhang, E. Kim, D. K. Mark, S. Choi, and O. Painter, A superconducting quantum simulator based on a photonic-bandgap metamaterial, *Science* **379**, 278 (2023).
- [18] B. Fauseweh, Quantum many-body simulations on digital quantum computers: State-of-the-art and future challenges, *Nat. Commun.* **15**, 2123 (2024).
- [19] C. Monroe, W. C. Campbell, L.-M. Duan, Z.-X. Gong, A. V. Gorshkov, P. W. Hess, *et al.*, Programmable quantum simulations of spin systems with trapped ions, *Rev. Mod. Phys.* **93**, 025001 (2021).
- [20] H. B. Kaplan, L. Guo, W. L. Tan, A. De, F. Marquardt, G. Pagano, *et al.*, Many-body dephasing in a trapped-ion quantum simulator, *Phys. Rev. Lett.* **125**, 120605 (2020).
- [21] C.-C. J. Wang and J. K. Freericks, Intrinsic phonon effects on analog quantum simulators with ultracold trapped ions, *Phys. Rev. A* **86**, 032329 (2012).
- [22] G. Pagano, P. W. Hess, H. B. Kaplan, W. L. Tan, P. Richerme, P. Becker, *et al.*, Cryogenic trapped-ion system for large scale quantum simulation, *Quantum Sci. Technol.* **4**, 014004 (2018).
- [23] R. Ott, D. González-Cuadra, T. V. Zache, P. Zoller, A. M. Kaufman, and H. Pichler, Error-corrected fermionic quantum processors with neutral atoms, *Phys. Rev. Lett.* **135**, 090601 (2025).
- [24] K. J. Satzinger, Y.-J. Liu, A. Smith, C. Knapp, M. Newman, C. Jones, *et al.*, Realizing topologically ordered states on a quantum processor, *Science* **374**, 1237 (2021).
- [25] R. Acharya, D. A. Abanin, L. Aghababaie-Beni, I. Aleiner, T. I. Andersen, M. Ansmann, *et al.*, Quantum error correction below the surface code threshold, *Nature* **638**, 920 (2025).
- [26] D. Bluvstein, A. A. Geim, S. H. Li, S. J. Evered, J. P. Bonilla Ataides, G. Baranes, *et al.*, A fault-tolerant neutral-atom architecture for universal quantum computation, *Nature* **649**, 39 (2026).
- [27] A. Rodriguez-Blanco, F. Shahandeh, and A. Bermudez, Witnessing entanglement in trapped-ion quantum error correction under realistic noise, *Phys. Rev. A* **109**, 052417 (2024).
- [28] F. Butt, I. Pogorelov, R. Freund, A. Steiner, M. Meyer, T. Monz, *et al.*, Demonstration of measurement-free universal logical quantum computation, *Nat. Commun.* [10.1038/s41467-026-68533-x](https://doi.org/10.1038/s41467-026-68533-x) (2026).
- [29] F. Arute, K. Arya, R. Babbush, D. Bacon, J. C. Bardin, R. Barends, *et al.*, Quantum supremacy using a programmable superconducting processor, *Nature* **574**, 505 (2019).
- [30] M. Saffman, T. G. Walker, and K. Mølmer, Quantum information with rydberg atoms, *Rev. Mod. Phys.* **82**, 2313 (2010).
- [31] T. F. Gallagher, *Rydberg Atoms*, Cambridge Monographs on Atomic, Molecular and Chemical Physics (Cambridge University Press, 1994).
- [32] M. Endres, H. Bernien, A. Keesling, H. Levine, E. R. Anschuetz, A. Krajenbrink, *et al.*, Atom-by-atom assembly of defect-free one-dimensional cold atom arrays, *Science* **354**, 1024 (2016).
- [33] C. S. Adams, J. D. Pritchard, and J. P. Shaffer, Rydberg atom quantum technologies, *J. Phys. B: At. Mol. Opt. Phys.* **53**, 012002 (2019).
- [34] M. Saffman, Quantum computing with atomic qubits and rydberg interactions: progress and challenges, *J. Phys. B: At. Mol. Opt. Phys.* **49**, 202001 (2016).
- [35] S. K. Barik, A. Thakur, Y. Jindal, S. B. S, and S. Roy, Quantum technologies with rydberg atoms, *Front. Quantum Sci. Technol.* **3**, 1426216 (2024).
- [36] M. Morgado and S. Whitlock, Quantum simulation and computing with rydberg-interacting qubits, *AVS Quantum Sci.* **3**, 023501 (2021).
- [37] M. Kim, K. Kim, J. Hwang, E.-G. Moon, and J. Ahn, Rydberg quantum wires for maximum independent set problems, *Nature Physics* **18**, 755 (2022).
- [38] H. Pichler, S.-T. Wang, L. Zhou, S. Choi, and M. D. Lukin, Quantum optimization for maximum independent set using rydberg atom arrays (2018), [arXiv:1808.10816](https://arxiv.org/abs/1808.10816).
- [39] C. Dalyac, L.-P. Henry, M. Kim, J. Ahn, and L. Henriot, Exploring the impact of graph locality for the resolution of the maximum-independent-set problem with neutral atom devices, *Phys. Rev. A* **108**, 052423 (2023).
- [40] A. Byun, M. Kim, and J. Ahn, Finding the maximum independent sets of platonic graphs using rydberg atoms, *PRX Quantum* **3**, 030305 (2022).
- [41] K. Kim, M. Kim, J. Park, A. Byun, and J. Ahn, Quantum computing dataset of maximum independent set problem on king lattice of over hundred rydberg atoms, *Sci. Data* **11**, 111 (2024).
- [42] J. Park, S. Jeong, M. Kim, K. Kim, A. Byun, L. Vignoli, *et al.*, Rydberg-atom experiment for the integer factorization problem, *Phys. Rev. Res.* **6**, 023241 (2024).
- [43] Y. Song, M. Kim, H. Hwang, W. Lee, and J. Ahn, Quantum simulation of cayley-tree ising hamiltonians with three-dimensional rydberg atoms, *Phys. Rev. Res.* **3**, 013286 (2021).
- [44] A. Byun, J. Jung, K. Kim, M. Kim, S. Jeong, H. Jeong, *et al.*, Rydberg-atom graphs for quadratic unconstrained binary optimization problems, *Adv Quantum Technol.* **7**, 2300398 (2024).
- [45] A. G. de Oliveira, E. Diamond-Hitchcock, D. M. Walker, M. T. Wells-Pestell, G. Pelegrí, C. J. Picken, *et al.*, Demonstration of weighted-graph optimization on a rydberg-atom array using local light shifts, *PRX Quantum* **6**, 010301 (2025).

- [46] S. Jeong, J. Park, and J. Ahn, Quantum-enhanced simulated annealing using rydberg atoms, *Adv. Quantum Technol.* **8**, e2500070 (2025).
- [47] S. Jansen, M.-B. Ruskai, and R. Seiler, Bounds for the adiabatic approximation with applications to quantum computation, *J. Math. Phys.* **48**, 102111 (2007).
- [48] A. Braidia, S. Chakraborty, A. Chaudhuri, J. Cunningham, R. Menavlikar, L. Novo, *et al.*, Unstructured Adiabatic Quantum Optimization: Optimality with Limitations, *Quantum* **9**, 1790 (2025).
- [49] E. Mozgunov and D. A. Lidar, Quantum adiabatic theorem for unbounded hamiltonians with a cutoff and its application to superconducting circuits, *Philos. Trans. A. Math. Phys. and Eng. Sci.* **381**, 20210407 (2022).
- [50] Q. Zhang, N. N. Hegade, A. G. Cadavid, L. Lassablière, J. Trautmann, S. Perseguers, *et al.*, Analog counterdiabatic quantum computing (2024), arXiv:2405.14829.
- [51] W. T. Hsieh and D. Sels, Less is more: subspace reduction for counterdiabatic driving of rydberg atom arrays (2025), arXiv:2512.04494.
- [52] S. Perseguers, Hardness-dependent quantum adiabatic schedules for the maximum-independent-set problem, *Phys. Rev. Appl.* **23**, 064023 (2025).
- [53] J. R. Finžgar, M. J. A. Schuetz, J. K. Brubaker, H. Nishimori, and H. G. Katzgraber, Designing quantum annealing schedules using bayesian optimization, *Phys. Rev. Res.* **6**, 023063 (2024).
- [54] B. F. Schiffer, D. S. Wild, N. Maskara, M. Cain, M. D. Lukin, and R. Samajdar, Circumventing superexponential runtimes for hard instances of quantum adiabatic optimization, *Phys. Rev. Res.* **6**, 013271 (2024).
- [55] J. Wurtz, A. Bylinskii, B. Braverman, J. Amato-Grill, S. H. Cantu, F. Huber, A. Lukin, F. Liu, P. Weinberg, J. Long, S.-T. Wang, N. Gemelke, and A. Keesling, Aquila: Quera's 256-qubit neutral-atom quantum computer (2023), arXiv:2306.11727.
- [56] S. de Léséleuc, D. Barredo, V. Lienhard, A. Browaeys, and T. Lahaye, Analysis of imperfections in the coherent optical excitation of single atoms to rydberg states, *Phys. Rev. A* **97**, 053803 (2018).

Appendix A: Derivation of the Two-Level Adiabatic Hamiltonian

Here we present the detailed derivation of the adiabatic Hamiltonian in Eq. (2), based on Theorem 1 of Ref. [47]. This theorem states that the upper bound on the population leakage from the ground state scales as $\varepsilon_{P_{E_0}}(s) = O(\tau^{-2})$, where $s \equiv t/\tau$ denotes the normalized evolution time and τ represents the characteristic time scale of the adiabatic evolution.

Let $W(s) \equiv |E_0(s)\rangle \langle E_0(s)|$ denotes the projection onto the ground state. The adiabatic Hamiltonian can be defined as

$$H_\tau^A(s) \equiv H(s) - \frac{i}{\tau} \left[\dot{W}(s), W(s) \right]. \quad (\text{A1})$$

Based on the energy spectrum $\{E_j\}$ of the Rydberg Hamiltonian H_{Ry} in Eq. (1), H can be written as

$$H(s) = \sum_j E_j(s) |E_j(s)\rangle \langle E_j(s)| \stackrel{\text{Diag}}{=} E_1(s) - \Delta E_{01}(s) \cdot W(s), \quad (\text{A2})$$

where $\stackrel{\text{Diag}}{=}$ indicates that the left- and right-hand sides differ only by a scalar multiple of the identity operator.

From the Eqs. (A1) and (A2),

$$H_\tau^A(s) = \sum_j E_j(s) |E_j(s)\rangle \langle E_j(s)| - \frac{i}{\tau} \left[\frac{d}{ds} |E_0(s)\rangle \langle E_0(s)|, |E_0(s)\rangle \langle E_0(s)| \right] \quad (\text{A3a})$$

$$= \sum_j E_j(s) |E_j(s)\rangle \langle E_j(s)| - \frac{i}{\tau} \left[\frac{d}{ds} |E_0(s)\rangle \cdot \langle E_0(s)| - |E_0(s)\rangle \cdot \frac{d}{ds} \langle E_0(s)| \right] \quad (\text{A3b})$$

$$= \sum_j E_j(t) |E_j(t)\rangle \langle E_j(t)| - i \left[\frac{d}{dt} |E_0(t)\rangle \cdot \langle E_0(t)| - |E_0(t)\rangle \cdot \frac{d}{dt} \langle E_0(t)| \right] \quad (\text{A3c})$$

$$\approx E_0(t) |E_0(t)\rangle \langle E_0(t)| + E_1(t) |E_1(t)\rangle \langle E_1(t)| - i \left[\frac{d}{dt} |E_0(t)\rangle \cdot \langle E_0(t)| - |E_0(t)\rangle \cdot \frac{d}{dt} \langle E_0(t)| \right], \quad (\text{A3d})$$

and

$$\dot{H}(s) = \sum_j \left[\dot{E}_j(s) |E_j(s)\rangle \langle E_j(s)| + E_j(s) \cdot \left\{ \frac{d}{ds} |E_j(s)\rangle \cdot \langle E_j(s)| + |E_j(s)\rangle \cdot \frac{d}{ds} \langle E_j(s)| \right\} \right] \quad (\text{A4a})$$

$$\approx \dot{E}_1(s) - \frac{d}{ds} [\Delta E_{01}(s)] \cdot W(s) - \Delta E_{01}(s) \cdot \dot{W}(s). \quad (\text{A4b})$$

From the Eqs. (A2), (A3) and (A4),

$$H_\tau^A(s = t/\tau) \approx E_0(t) |E_0(t)\rangle \langle E_0(t)| + E_1(t) |E_1(t)\rangle \langle E_1(t)| - \frac{i}{\tau \Delta E_{01}(s)} \left[\dot{E}_1(s) - \frac{d}{ds} [\Delta E_{01}(s)] \cdot W(s) - \dot{H}(s), W(s) \right] \quad (\text{A5a})$$

$$= E_1(s) - \Delta E_{01}(s) \cdot W(s) + \frac{i}{\tau \Delta E_{01}(s)} \left[\dot{H}(s), W(s) \right] \quad (\text{A5b})$$

Comparing the Eqs. (A1), (A2) and (A5b),

$$W(s) \stackrel{\text{Diag}}{=} -\frac{H(s)}{\Delta E_{01}(s)}, \quad \dot{W}(s) \stackrel{[W(s), \cdot]}{=} \frac{\dot{H}(s)}{\Delta E_{01}(s)}, \quad (\text{A6})$$

where $\stackrel{[W(s), \cdot]}{=}$ indicates that the two sides are equivalent when evaluated within the commutator $[W(s), \cdot]$. This leads to H_{ad} (Eq. (2)):

$$H_\tau^A(s = t/\tau) \stackrel{\text{Diag}}{=} \frac{\langle E_1 | \frac{dH}{dt} | E_0 \rangle}{\Delta E_{01}} s_y - \frac{\Delta E_{01}}{2} s_z [\equiv H_{\text{ad}}(t)]. \quad (\text{A7})$$

Appendix B: Atomic Coordinates for the Quasi-One-Dimensional Chains and Two-Dimensional Triangular Lattices

TABLE I. Atom positions of $Q_{1D,10}$

Graph	Atom positions (x, y) (μm)
$Q_{1D,10}$	$x_1: (6.93, 8.00)$ $x_2: (20.78, 8.00)$
	$x_3: (34.64, 8.00)$ $x_4: (0.00, 4.00)$
	$x_5: (13.85, 4.00)$ $x_6: (27.71, 4.00)$
	$x_7: (41.57, 4.00)$ $x_8: (6.93, 0.00)$
	$x_9: (20.78, 0.00)$ $x_{10}: (34.64, 0.00)$

TABLE II. Atom positions of $T_{D,25}$, $T_{H,37}$

Graph	Atom positions (x, y) (μm)	Graph	Atom positions (x, y) (μm)
$T_{D,25}$	$x_1: (27.71, 4.00)$	$T_{H,37}$	$x_1: (20.78, 0.00)$
	$x_3: (34.64, 8.00)$		$x_2: (13.86, 4.00)$
	$x_5: (27.71, 12.00)$		$x_3: (27.71, 4.00)$
	$x_7: (6.93, 16.00)$		$x_4: (6.93, 8.00)$
	$x_9: (34.64, 16.00)$		$x_5: (20.78, 8.00)$
	$x_{11}: (0, 20.00)$		$x_6: (34.64, 8.00)$
	$x_{13}: (27.71, 20.00)$		$x_7: (0.00, 12.00)$
	$x_{15}: (55.43, 20.00)$		$x_8: (13.86, 12.00)$
	$x_{17}: (20.78, 24.00)$		$x_9: (27.71, 12.00)$
	$x_{19}: (48.50, 24.00)$		$x_{10}: (41.57, 12.00)$
	$x_{21}: (27.71, 28.00)$		$x_{11}: (6.93, 16.00)$
	$x_{23}: (20.78, 32.00)$		$x_{12}: (20.78, 16.00)$
	$x_{25}: (27.71, 36.00)$		$x_{13}: (34.64, 16.00)$
			$x_{14}: (0.00, 20.00)$
			$x_{15}: (13.86, 20.00)$
	$x_{16}: (27.71, 20.00)$		
	$x_{17}: (41.57, 20.00)$		
	$x_{18}: (6.93, 24.00)$		
	$x_{19}: (20.78, 24.00)$		
	$x_{20}: (34.64, 24.00)$		
	$x_{21}: (0.00, 28.00)$		
	$x_{22}: (13.86, 28.00)$		
	$x_{23}: (27.71, 28.00)$		
	$x_{24}: (41.57, 28.00)$		
	$x_{25}: (6.93, 32.00)$		
	$x_{26}: (20.78, 32.00)$		
	$x_{27}: (34.64, 32.00)$		
	$x_{28}: (0.00, 36.00)$		
	$x_{29}: (13.86, 36.00)$		
	$x_{30}: (27.71, 36.00)$		
	$x_{31}: (41.57, 36.00)$		
	$x_{32}: (6.93, 40.00)$		
	$x_{33}: (20.78, 40.00)$		
	$x_{34}: (34.64, 40.00)$		
	$x_{35}: (13.86, 44.00)$		
	$x_{36}: (27.71, 44.00)$		
	$x_{37}: (20.78, 48.00)$		

TABLE III. Atom positions of $Q'_{1D,23}$

Graph	Atom positions (x, y) (μm)
$Q'_{1D,23}$	$x_1: (13.86, 4.00)$
	$x_2: (20.78, 0.00)$
	$x_3: (27.71, 4.00)$
	$x_4: (34.64, 0.00)$
	$x_5: (41.57, 4.00)$
	$x_6: (48.50, 0.00)$
	$x_7: (55.43, 4.00)$
	$x_8: (6.93, 8.00)$
	$x_9: (20.78, 8.00)$
	$x_{10}: (34.64, 8.00)$
	$x_{11}: (48.50, 8.00)$
	$x_{12}: (6.93, 16.00)$
	$x_{13}: (6.93, 24.00)$
$x_{14}: (13.86, 28.00)$	
$x_{15}: (20.78, 24.00)$	
$x_{16}: (27.71, 28.00)$	
$x_{17}: (34.64, 24.00)$	
$x_{18}: (41.57, 28.00)$	
$x_{19}: (48.50, 24.00)$	
$x_{20}: (55.43, 28.00)$	
$x_{21}: (20.78, 32.00)$	
$x_{22}: (34.64, 32.00)$	
$x_{23}: (48.50, 32.00)$	